Available online at www.sciencedirect.com
SCIENCE DIRECT®
Pattern Recognition 38 (2005) 2639–2652
PATTERN RECOGNITION
THE JOURNAL OF THE PATTERN RECOGNITION SOCIETY
www.elsevier.com/locate/patcog

Palmprint verification using hierarchical decomposition

Chih-Lung Lin[a], Thomas C. Chuang[b,*], Kuo-Chin Fan[c]

[a]*Department of Electronic Engineering, Tung Nan Institute of Technology, ShenKeng, Taipei, 222, Taiwan, ROC*
[b]*Department of Computer Science and Information Engineering, Vanung University, Jhong-Li, Tao-Yuan, Taiwan, ROC*
[c]*Department of Computer Science and Information Engineering, National Central University, Jhong-Li, Tao-Yuan, Taiwan, ROC*

Received 4 June 2004; received in revised form 12 April 2005; accepted 12 April 2005

Abstract

A reliable and robust personal verification approach using palmprint features is presented in this paper. The characteristics of the proposed approach are that no prior knowledge about the objects is necessary and the parameters can be set automatically. In our work, a flatbed scanner is adopted as an input device for capturing palmprint images; it has the advantages of working without palm inking or a docking device. In the proposed approach, two finger-webs are automatically selected as the datum points to define the region of interest (ROI) in the palmprint images. The hierarchical decomposition mechanism is applied to extract principal palmprint features inside the ROI, which includes directional and multi-resolution decompositions. The former extracts principal palmprint features from each ROI. The latter process the images with principal palmprint feature and extract the dominant points from the images at different resolutions. A total of 4800 palmprint images were collected from 160 persons to verify the validity of the proposed palmprint verification approach and the results are satisfactory with acceptable accuracy (FRR: 0.75% and FAR: 0.69%). Experimental results demonstrate that our proposed approach is feasible and effective in palmprint verification.

Keywords: Palmprint verification; Finger-web; Template matching; Correlation function; Kalman predictor

1. Introduction

Due to the explosive growth and popularity of the Internet in recent years, an increasing number of security access control systems based on personal verifications have been presented recently. Traditional personal verification methods rely heavily on the use of passwords, personal identification numbers (PINs), magnetic swipe cards, keys, smart cards, etc. No matter which method is employed, it offers only limited security. Many biometric verification techniques dealing with various human physiological features including facial images, hand geometry, fingerprint and retina pattern [1] have been proposed to improve the security of personal verification. In addition, the infrared imagings of biological features, such as the infrared images of faces [1,2] and subcutaneous vascular network on the back of hands, have also been investigated [3]. Some factors that may affect the popularity, performance and applicability of biometric verification techniques are uniqueness, repeatability, immunity to forgery, operation under controlled light or not, invasiveness or non-invasiveness, identification of dark-skinned objects, throughput rate, false rejection rate (FRR) and false acceptance rate (FAR), user cooperation, ease of use and cleanliness. Recently, there is still no biometric verification technique that can satisfy all these needs [4].

In this paper, we present a novel palmprint verification method for personal identification. In general, palmprints consist of some significant textures and a lot of minutiae similar to the creases, ridges and branches of fingerprints. In addition, there are many different features existing in

* Corresponding author. Tel.: 886 3 451 5811x279; fax: 886 3 451 3786.
E-mail address: tomchuang@msa.vnu.edu.tw (T.C. Chuang).

0031-3203/$30.00
doi:10.1016/j.patcog.2005.04.001

palmprint images, such as the geometry, the principal line, the delta point, wrinkle features, etc. [9,14]. Both palmprint and fingerprint offer stable, unique and repeatable features for personal identification which have been used for criminal verification by law enforcement agents for more than 100 years [9].

However, it is a difficult task to extract small unique features (known as minutiae) from the fingers of elderly people as well as manual laborers [5,6]. Using a high-resolution input device in acquiring minutia images is the solution to remedy this problem. Many verification technologies using biometric features of palms were developed recently [7–16]. Han et al. [7] used the generalized learning vector quantization (GLVQ) approach to verify the identity of persons. Lin et al. [8] accomplished the verification by using a fuzzy inference engine. Zhang and Shu [9] transferred the palmprints to line sections to verify palmprint features. Chen et al. [10] compared the directions of crease pixels to recognize the palmprints. Kong and Zhang [11] used Hamming distance of texture information, using a 2-D Gabor filter, for verification. Wu et al. [12] used the fuzzy directional element energy feature (FDEEF) to identify palmprints. Duta et al. [13] extracted a set of feature points along palm lines and computed a matching score between the corresponding sets of feature points of the two palmprints. You et al. [14] used the global texture energy of palmprints for the verification. Lu et al. [15] applied the eigenpalms and the Euclidean distance classifier to recognize palmprints. Han et al. [16] used a neural network to verify the identity of persons. However, all these methods require a docking device to constrain the palm position [7,8,10,11] or the palm to be inked [9,13,14,17] while acquiring palmprint images. Moreover, there is often a concave region at the palm center of the average person. This property will generate a white center region on the inked palmprint images and will inevitably cause the loss of important information about the center region of the palmprint images (see the figures in [9,14,17]). Although Kumar et al. [18] had developed a method to conquer these drawbacks by using a digital camera to capture palmprint images; the system setup was relatively bulky, complex and costly. In this paper, we propose another approach to overcome thesedrawbacks while maintaining the accuracy of palmprint verification. The overall system is compact and simple; the scanning quality is more consistent and uniform. We developed a compact, reliable and robust system that relies on principal lines and wrinkles of palmprints without needing a docking device or palm inking. Both principal lines and wrinkles of palmprints are named principal palmprints in the following contexts.

The rest of this paper is organized as follows. We will briefly introduce the palmprint image collection device and process in Section 2. The preprocessing and segmentation methods are addressed in Section 3. Section 4 illustrates the procedures for the determination of finger-web locations and the location of region of interest (ROI). Section 5 describes the methods of hierarchical decomposition to extract the principal palmprint features and dominant points. The construction of a template library is presented in Section 6. The verification algorithm is stated in Section 7. Experimental results are demonstrated in Section 8 to verify the validity of the proposed approach. Finally, concluding remarks are given in Section 9.

A block diagram of the proposed approach is shown in Fig. 1. Firstly, the palmprint images are captured by a flatbed scanner as the input data. Then, a median filter is employed on the palmprint images to remove system noise and a mode method is applied to select a suitable threshold to segment a palm region. The four finger-web locations are found automatically and a square ROI is obtained accordingly based on the second and fourth finger-webs. Next, principal palmprint features within each ROI are extracted by directional decomposition. Multi-resolution representations of the images with extracted principal palmprint features are obtained by using a multi-resolution filter (MRF) that extracts dominant points. Finally, a normalized correlation function is adopted to verify whether the template and testing samples are captured from the same person or not.

2. Palmprint images collection

A flatbed scanner, as a popular PC peripheral device, was used to acquire palmprint images. It possesses the benefits of high availability, uniform and consistent good image quality, convenience and low cost. In this work, the scanner that we used to acquire palmprint images was a UMAX VISTA-S6 as shown in Fig. 2. The resolution of the scanner was set at 100 dpi with 8 bit gray-scales per pixel. The reason for using such a low spatial resolution is that both the data amount of palmprint images and noise sensitivities can be reduced while the features of principal palmprints can still be preserved [9]. To reduce the image size, a square area on the surface of the scanning region is set with its dimension being a little larger than that of a person's palm. The advantages of this scanning manner are that the palms need not to be inked and no docking device is required on the scanner to constrain the palm position as shown in Fig. 2. Thus, there is tolerable space available for positioning and rotating the palm within the specified square region. To obtain high verification accuracy, it is important to construct an objective verification template library. Therefore, 160 persons were enrolled in our study and the palmprint images were captured from their right hands at three different times at an interval of at least one week. Ten palmprint images were acquired each time for each person. The template library constructed in this way includes possible variations of palmprint images under various conditions. The sample group was selected for a particular security system application for offices and schools. The 160 palmprints collected are therefore associated with office workers or students of the age group of 18–26 year old. There was not a specific distinction between male and female when the samples were collected.

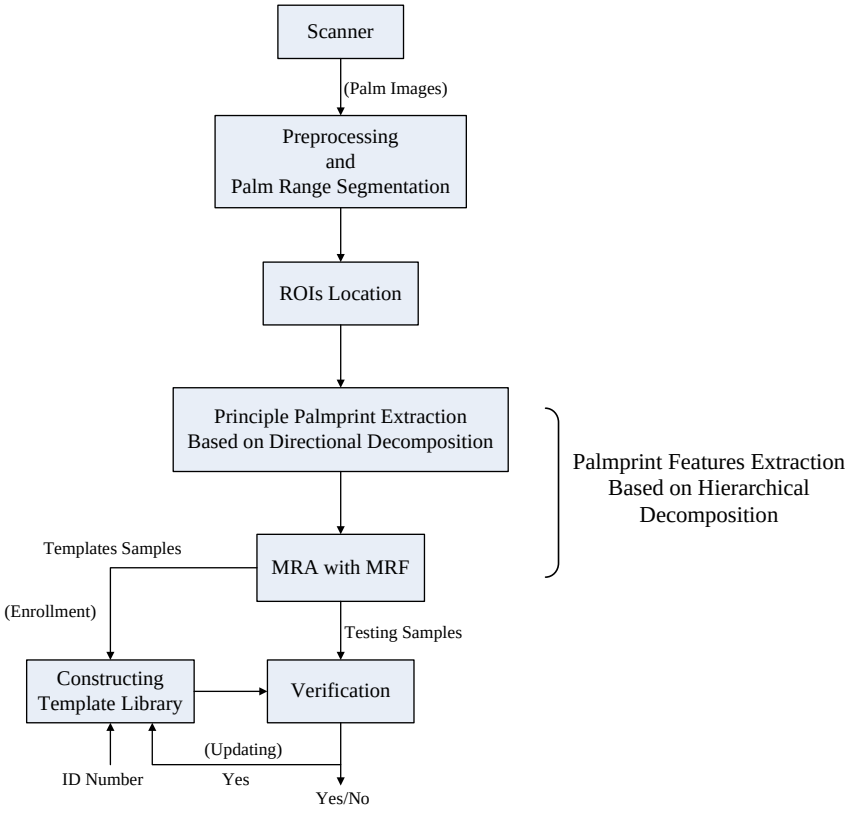

Fig. 1. Block diagram of the approach.

Fig. 2. The flatbed scanner is utilized to capture the palmprint images. The palms need not be inked and no docking device is required on the scanner to constrain the palm position while acquiring palmprint images.

3. Preprocessing and segmentation

As we know, flatbed scanners are very mature PC peripheral products. The images captured by these scanners have high quality and low noise. As shown in Fig. 3 , the palmprint images are captured with little noises by the scanner. Traditional median filter can be utilized to reduce noise effectively. By carefully analyzing the histograms of palmprint images, we find that the histograms are typically bimodal as shown in Fig. 4(b). Hence, we adopt a mode method [23] to determine the suitable threshold in binarizing palmprint images. It is clear that there are many empty bins in the histograms. We can fill these empty bins by linear interpolation. The mode method first finds the local maximums, $P1$ and $P2$, (Eq. (1)) and then detects the local minimum B (Eq. (2)) as the threshold between the two local maximums in the histogram as shown in Fig. 4(b).

$$P = \left\{ n | G(n) = \max_{i=-l}^{l} G(n+i) \right\}, \tag{1}$$

$$B = \left\{ n | G(n) = \min_{i=-l}^{l} G(n+i) \right\}, \tag{2}$$

where P is the gray level of the local maximum in the histogram, B is the gray level of the local minimum in the histogram, n is the gray level, $G(n)$ is the number of pixels whose gray level is n and $2l+1$ is equal to the window size.

The selected threshold is utilized to segment the image. The result is a binary palmprint image as shown in Fig. 4(c).

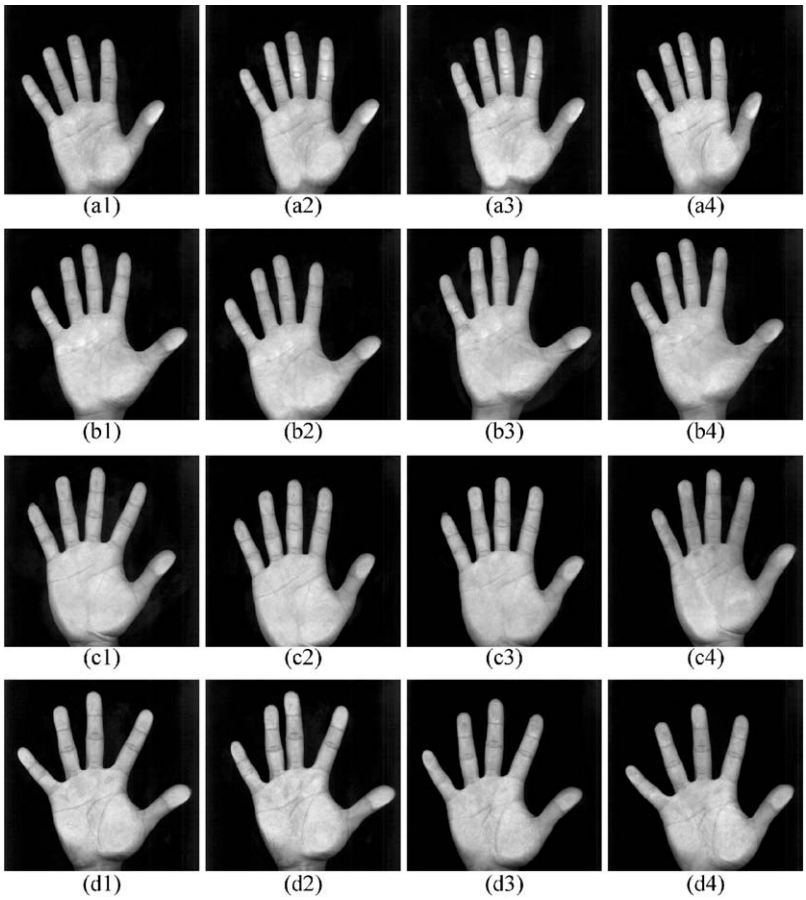

Fig. 3. The original gray-level images of palmprint captured from four different persons by flatbed scanner. (a1)–(a4) are captured from the same person. Similarly, (b1)–(b4), (c1)–(c4) and (d1)–(d4) are captured from three different persons, respectively.

By comparing the segmented palm shapes with those of original palm images, we can discover that they are almost indistinguishable as shown in Fig. 4(a) and (c). It shows that the mode method is quite effective in determining the threshold of palmprint images.

4. Region of interest location

To increase the verification accuracy and reliability, we compare the principal palmprint features extracted from the same region in different palmprint images for each verification. The region to be extracted is known as the ROI. For this reason, it is important to fix the ROI at the same position in different palmprint images to ensure the stability of the extracted principal palmprint features. However, it is difficult to fix the ROI at the same position in different palmprint images without any docking devices to constrain the palm position while acquiring palmprint images.

There are many researches [7–16] conducted on palmprint recognition. Except for [13], all of these methods verified the palmprint features extracted from the square region (ROI) of palmprint images. The methods introduced in [7,8] applied a docking device to constrain the palm position. The schemes addresseded in [10,12,15] did not discuss how to locate the ROI. The method proposed in [9,14] locates the ROI based on two end points which can be obtained from the intersections of principal lines with the two sides of the palm. Kong and Zhang [11] located the ROI according to finger-webs. Han et al. [16] applied the central line of medius as the reference to define ROI. Li et al. [17] introduced the direction of palm outer boundary and end point of heart line to deal with the rotation and shift of images. The techniques proposed in [9,14,17] do not need a docking device, but they have to process inked images. The methods of location ROI developed in [11,16] can obtain acceptable results without the need of docking devices or inked palmprint images. However, the medius utilized in [16] is movable over a certain range which will result in the shifting or rotating of the ROI in a small range. In [11], the palmprint images must contain three holes between the four fingers on the left which limits the range of palm rotation and shift while

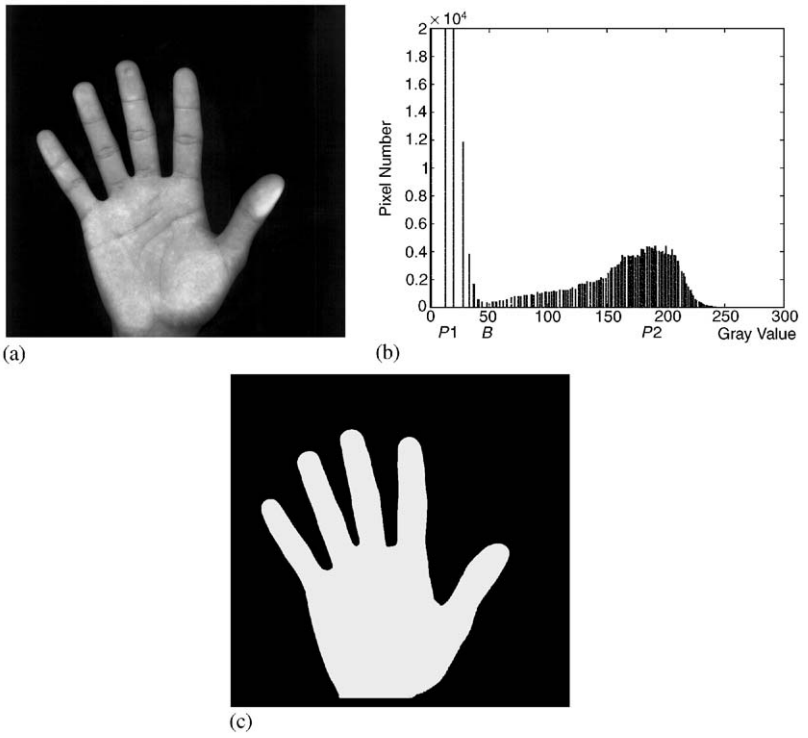

Fig. 4. The figures to demonstrate the effects of the threshold selected by the mode method. (a) An original gray-level image of palmprint is captured by the scanner. (b) The histogram of the palmprint image (a), the vertical and horizontal axes are pixel number and gray value, respectively. $P1$ and $P2$ are the positions of local maximums. B is the position of local minimum between two local maximums. B is selected as a threshold to segment the palm region. (c) The palm region is segmented by the threshold B which is selected by the mode method.

acquiring palmprint images. To alleviate these drawbacks, a method which adopts finger-webs as the datum points is developed to determine the approximate (not absolute) immovable ROI in this paper. The proposed method possesses two significant advantages. The first is that it can reduce the displacement of the ROI to an acceptable range. The second is that the range of palm rotation and shift while acquiring palmprint images can be reduced. The details of the method are discussed in the following contexts.

4.1. Finger-webs location

The following processes are performed to locate finger-webs in binary palmprint images. First, the inner border tracing algorithm [23] is employed to find the palm border. The starting point is the bottom-left point *Ps* of the palm as shown in Fig. 5(a). The tracing direction is along the palm border in the counterclockwise direction until the starting point *Ps* is met again. There is no need to locate the separation line between the wrist and the palm. Fig. 5(b) is an example illustrating the extracted border of a palmprint image which perfectly matches the original palm outline. The border pixels can be collected into a vector called border-pixel-vector (BPV).

Next, the middle point (W_m) of the intersection line that is formed by the wrist and bottom margin of a palmprint image is located as shown in Fig. 5(a). With W_m and BPV coordinates being known, we can calculate the Euclidean distance $D_E(i)$ between W_m and BPV.

$$D_E(i) = \sqrt{(X_{wm} - X_b(i))^2 + (Y_{wm} - Y_b(i))^2}, \tag{3}$$

where (X_{wm}, Y_{wm}) is the coordinate of the wrist middle point W_m, $(X_b(i), Y_b(i))$ is the coordinate of the ith border pixel, and $D_E(i)$ is the Euclidean distance between the ith border pixel and the wrist middle point W_m.

A distance distribution diagram (see Fig. 6) can be constructed by $D_E(i)$. As can be seen, there are five local maximums and four local minimums. The pattern in the diagram is quite similar to the geometric shape of a palm (see Fig. 5), which also has five tips (local maximums) and four finger-webs (local minimums). Experimenting on a wide variety of palmprint images, we find that the four local minimum locations in the distance distribution diagram are the same as finger-web locations and they match each other very well by confirming their locations.

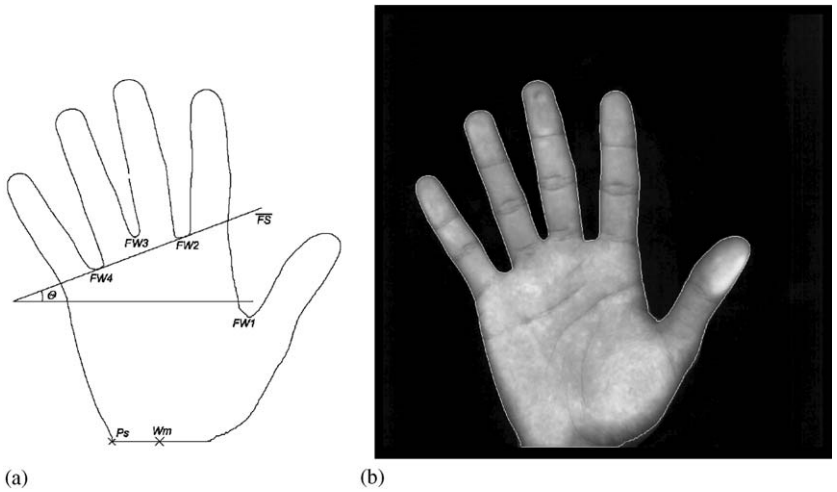

Fig. 5. The figures to demonstrate the effects of the inner border tracing algorithm. (a) The palm border is extracted by the inner border tracing algorithm. FW_1, FW_2, FW_3 and FW_4 represent the four finger-webs. $\overline{FS}$ represents the line traverses FW_2 and FW_4. θ is the include angle between $\overline{FS}$ and the horizontal. W_m is the middle point of wrist. *Ps* is the start point of the inner border tracing algorithm. (b) The border (white pixels) is superimposed the palm. It demonstrates that the border and the palm outline match well.

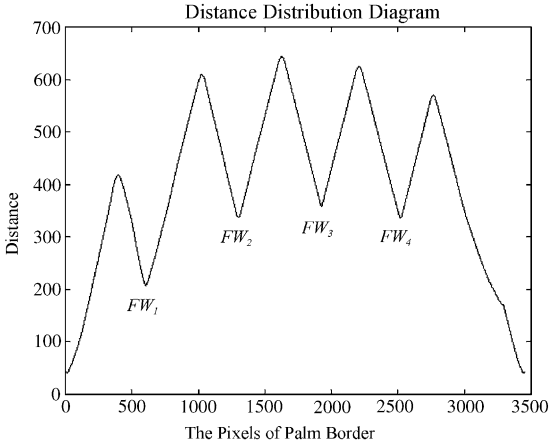

Fig. 6. The distance distribution diagram of the palm border. It is constructed by the Euclidean distances between palm border pixels and the middle point of wrist (W_m). FW_1, FW_2, FW_3 and FW_4 are the positions of four finger-webs.

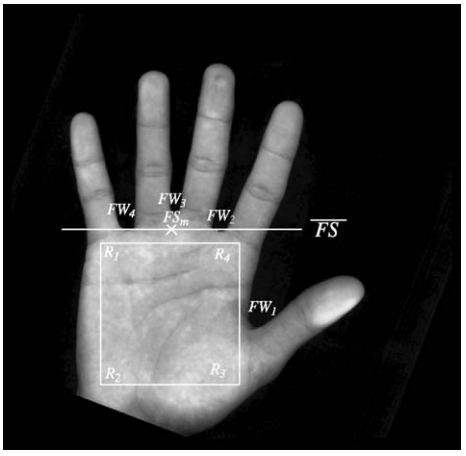

Fig. 7. The location of ROI is defined inside a palmprint image. FS_m is the middle point of FW_2 and FW_4. For convenience to define a square ROI, the palm is rotated θ to let FW_2 andFW_4 in the horizontal. According to FS_m location and $\overline{FS}$ direction, the region of a square ROI can be defined inside a palmprint image.

4.2. Region of interest location

In our work, the second and fourth finger-webs are selected as the datum points in location ROI. The former is between the forefinger and the medius, whereas the latter is between the ring and the little finger. They are denoted as FW_2 and FW_4, respectively, as shown in Fig. 5(a). FW_2 and FW_4 are then employed to locate the ROI. The procedure is described as follows.

First, the straight line $\overline{FS}$ is formed by finger-webs FW_2 and FW_4 as shown in Fig. 5(a). To eliminate the influences of palm rotation and define the coordinates of ROI more conveniently, the palmprint image is rotated an angle θ (Eq. (4)) which is between line $\overline{FS}$ and the horizontal line.

$$\theta = \tan^{-1}(Y_{FW_2} - Y_{FW_4})/(X_{FW_2} - X_{FW_4}), \tag{4}$$

where (X_{FW_2}, Y_{FW_2}) is the coordinate of FW_2 and (X_{FW_4}, Y_{FW_4}) is the coordinate of FW_4.

Therefore, the direction of line $\overline{FS}$ is horizontal and FS_m is the middle point between FW_2 and FW_4 on line $\overline{FS}$. A square region (256 × 256) whose corners are R_1, R_2, R_3

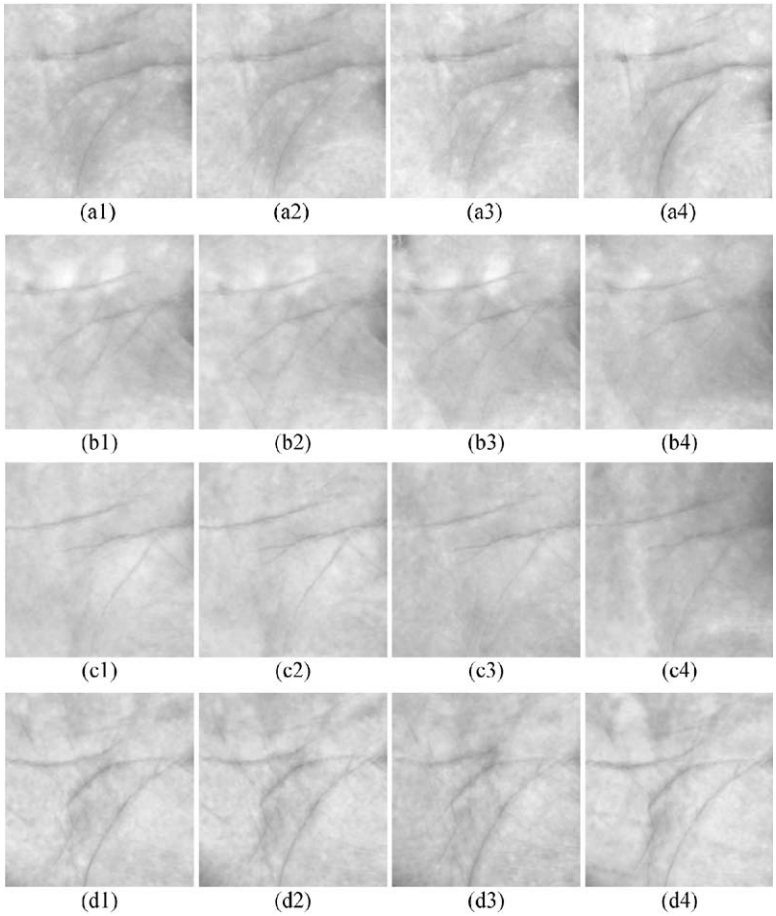

Fig. 8. The figures to demonstrate the effects of the proposed scheme which can automatically define the ROI. (a1)–(a4), (b1)–(b4), (c1)–(c4) and (d1)–(d4) are the ROIs extracted from the palm images shown in Fig. 3 (a1)–(a4), (b1)–(b4), (c1)–(c4) and (d1)–(d4), respectively. The ROI (a1)–(a4) extracted from the different palm images which are captured form one person almost cover the same region, and the ROI (b1)–(b4), (c1)–(c4) and (d1)–(d4) do likewise.

and R_4 is located and denoted as the ROI. Let the top side $\overline{R_1R_2}$ of the ROI be parallel to line $\overline{FS}$. The middle point of $\overline{R_1R_2}$ and FS_m are vertical and the distance between $\overline{R_1R_2}$ and FW_3 is half the width of the medius as shown in Fig. 7. Finally, we redefine the original coordinate (0,0) at the upper-left point R_1 of the ROI. Fig. 8 depicts the original palmprint images inside different ROIs captured from the same person. The results show that they are almost located at the same region. In this way, it can overcome the problem induced by not using docking devices while acquiring palmprint images. High verification accuracy can also be maintained simultaneously.

5. Principal palmprint features extraction based on hierarchical decomposition

The line segment is a significant feature to represent principal palmprints. It contains various crucial features, such as end point locations, directions, width, length and intensity. It is not surprising that these features cannot be effectively extracted by using only a single step. For example, the features seldom exist simultaneously in global-and-local regions, spatial-and-frequency domains, or gray-and-gradient scales. In order to alleviate such shortcomings, hierarchical decomposition is utilized in our work to effectively extract the various principal palmprint features. The hierarchical decomposition has been proven to be useful in many literatures [19–22]. It consists of two types of a directional decomposition and a multi-resolution analysis (MRA) processes.

5.1. Directional decomposition

By carefully observing palmprint images, we find that the principal palmprints possess low gray-level against background (skin of inner side of palm), whereas the minutiae

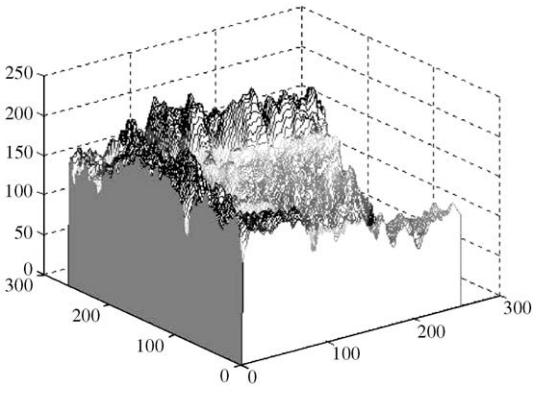

Fig. 9. The 3D profile of a ROI. The vertical axis represents the gray-level of pixels. The other two axes represent the coordinates of pixels. The profile demonstrates a sudden change in the gray-level of adjacent pixels near the principal palmprint, whereas the minutiae do not.

do not. A sudden change in the gray-level of adjacent pixels is found near the principal palmprints as shown in Fig. 9. Hence, the principal palmprints form quite distinctive features. In order to extract principal palmprint features and omit the minutiae in the ROI, we utilize the edge detector to extract the feature points of principal palmprint. An abundance of edge detection methods have been developed with good performance [23,25–28]. In order to maintain the information of edge directions while extracting edges, we apply the popular and mature Sobel operator to extract the edges of palmprints.

Firstly, let $\Phi_1(x, y)$, $\Phi_2(x, y)$, $\Phi_3(x, y)$ and $\Phi_4(x, y)$ be the four edge detectors of Sobel operator in 0°, 45°, 90° and 135° directions, respectively. The edges of an image $f(x, y)$ can be decomposed into four independent directions as follows:

$$F_n = f * \Phi_n, \tag{5}$$

where F_n is the decomposed image by Φ_n with the n direction, $n=1, 2, 3, 4$ represent the 0°, 45°, 90° and 135° directions, respectively, and * denotes the convolution operator.

$$\Phi_1 = \begin{bmatrix} 1 & 2 & 1 \\ 0 & 0 & 0 \\ -1 & -2 & -1 \end{bmatrix} \quad \Phi_2 = \begin{bmatrix} 2 & 1 & 0 \\ 1 & 0 & -1 \\ 0 & -1 & -2 \end{bmatrix} \quad \Phi_3 = \begin{bmatrix} 1 & 0 & -1 \\ 2 & 0 & -2 \\ 1 & 0 & -3 \end{bmatrix} \quad \Phi_4 = \begin{bmatrix} 0 & 1 & 2 \\ -1 & 0 & 1 \\ -2 & -1 & 0 \end{bmatrix}$$

Basically, there are four decomposed components that are equivalent to the gradient of $f(x, y)$ processed by Φ_n in the 0°, 45°, 90° and 135° directions. The F_n are thresholded by a preset value which will be described later to detect all the principal palmprints of $f(x, y)$.

To conquer the variations imposed by different images, a fixed threshold is not suitable. In this paper, we adopt the iterative threshold selection method [23] to segment the palmprint images (see Fig. 10(a1)–(a4)) which are processed by edge detectors. The procedure is stated as follows:

Step 1: Initialize the threshold $Th(1)(0 < Th(1) < 255)$ to segment the image into the background and the object.

Step 2: At kth iteration, compute $\mu_B(k)$ and $\mu_o(k)$ as the means of background and object gray-level, respectively. The threshold $Th(k)$ adopted in segmenting images into the background and the object is determined in step 3 of previous iteration (Eq. (8)).

$$\mu_B = \sum_{(i,j)\in background} f(i, j)/N_B, \tag{6}$$

$$\mu_o = \sum_{(i,j)\in object} f(i, j)/N_o, \tag{7}$$

where N_B and N_o are the pixel numbers of the background and the object, respectively.

$$Step\ 3\text{: Set } Th(k+1) = (\mu_B(k) + \mu_o(k))/2 \tag{8}$$

$Th(k+1)$ is the new threshold for the next iteration.

Step 4. If $Th(k+1) = Th(k)$, then terminate; otherwise return to step 2.

The processed images F_n are transformed into binary images by following these steps. We extract principal palmprints in binary images, sequential morphological operators are then employed which include majority, clean and dilation operations to trim the short principal palmprint lines. The trimmed images that only include principal palmprints are called principal palmprint images (PPIs) as shown in Fig. 10(c1)–(c4). It reveals that the application of edge detector, iterative threshold selection and sequential morphological operators can achieve good performance in feature extraction by comparing the PPIs (see Fig. 10(c1)–(c4)) with the original palmprint images inside the ROI (see Fig. 8(a1)).

5.2. Multi-resolution analysis with multi-resolution filter

MRA of signals has proven effective at extracting local features [24]. In addition, a multi-resolution representation provides a simple hierarchical framework for interpreting image information [29]. The information at different resolutions in an image generally represents different physical structures in the image. In the literature a number of applications of multi-resolution representations in image analysis have been discussed [14,30–32].

Although the ROI has been carefully located, it still cannot guarantee that the location of every pixel representing the principal palmprint is always at the same position in different ROIs of the same palm. To resolve this problem, we apply the MRA to decompose the PPI into multi-scale PPIs. Let us call them subPPIs in the following contexts. The fine resolution images effectively provide us the ability to watch an object at closer distances which reveals detailed information that is more sensitive to disturbances and noises.

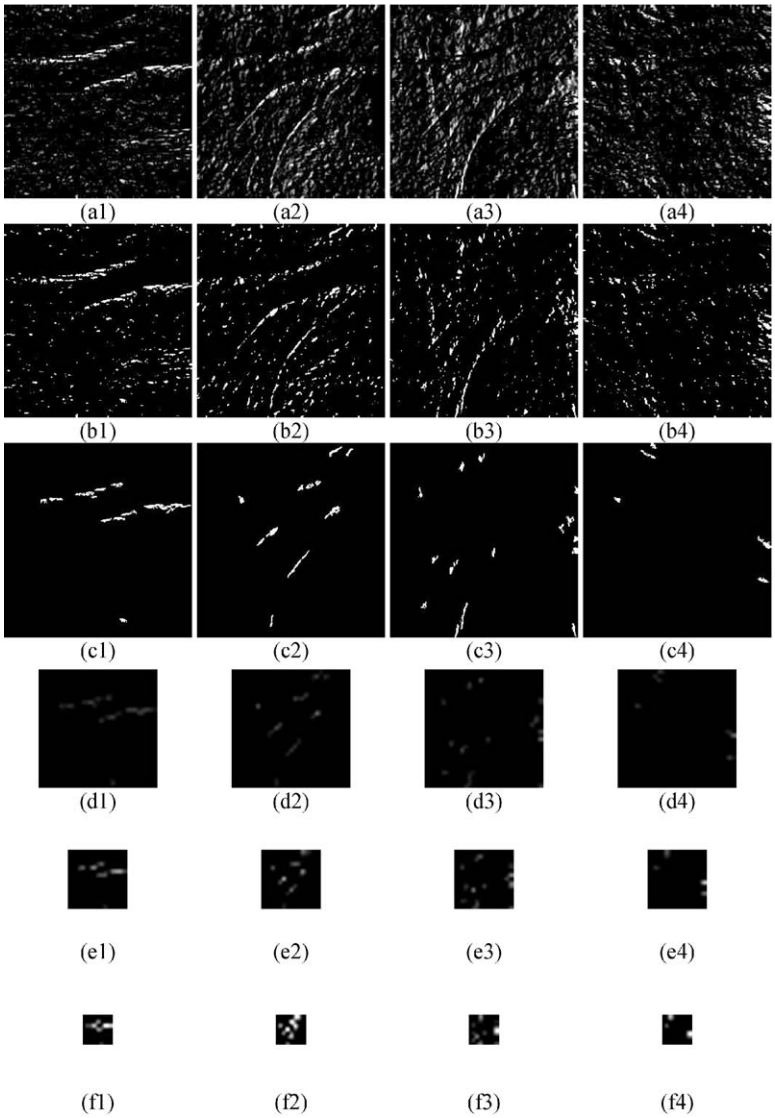

Fig. 10. The figures to demonstrate the procedures of extracting principal palmprints. The principal palmprint images (PPIs) are extracted from Fig. 8 (a1). (a1)–(a4) are the results processed by four edge detectors. They represent the 0°, 45°, 90°, and 135° directions, respectively. In order to observe easily, they are normalized in gray-level. (b1)–(b4) are the binary images segmented by the optimal threshold. (c1)–(c4) are the images processed by sequential morphological operators to trim the short palmprint lines. They only contain the principal palmprints. (d1)–(d4), (e1)–(e4) and (f1)–(f4) exhibit the dominant points at the 3rd, 4th and 5th level subPPIs, respectively. In order to observe conveniently, their scales are enlarged with four times and intensities are duple. They demonstrate the advantage which the scale is reduced, the intensity of dominant points is increased. While reducing the scale, the dominant points aggregate the strength, location and directions information about the neighboring feature points but not discard them.

On the contrary, a coarser resolution image is viewed as if watching an object far away which possesses gross information and is less sensitive to disturbances and noises.

Abundant multi-resolution filters have been described in the literature. They can be categorized into two groups: linear filters and nonlinear filters [30]. The characteristic of MRFs is that they will directly discard the pixels while doing down sampling. If the discarded pixels happen to be feature points, it will unfortunately result in the loss of the significant information of biometric features at the next resolution level. To remedy this problem, we propose a sum operator as a MRF to filter the dominant points that construct multi-scale images. For convenience, this MRF is called a dominant point filter in the following contexts. There are two main advantages of using the dominant point filter. Firstly, it aggregates the information of neighboring dominant points

at the previous resolution level to construct the next resolution level instead of discarding them directly. This is quite different from the approach of using wavelet transformation (WT) [24] for the multi-resolution local analysis of signals. Each dominant point aggregates the strength, location and direction information of the neighboring points of principal palmprint features at the previous resolution level as shown in Fig. 10(d1–d4, e1–e4 and f1–f4). They are used to construct the template library for palmprint verification. Secondly, it can also reduce the data amount of the template and decrease the computation load. For example, it can reduce 256×256 to 32×32, 16×16 and 8×8 at the 3rd, 4th and 5th levels, respectively. The dominant point filter will construct the following new subPPIs recursively.

$$p^{(m+1,n)}(x, y) = sum(p^{(m,n)}(2x, 2y), p^{(m,n)}(2x+1, 2y), p^{(m,n)}(2x+1, 2y+1), p^{(m,n)}(2x, 2y+1)), \quad (9)$$

where $p^{(m,n)}(x, y)$ is the dominant points with the n direction at the mth level subPPI, $n = 1, 2, 3, 4$ represent the 0°, 45°, 90° and 135° directions, respectively, and $p^{(0,n)}(x, y)$ represents the palmprint feature point in original PPI.

6. Template library construction

In our work, two stages are executed to construct the template library. They are described as follows.

(1) *Enrollment stage*: it is used for persons without any palmprint template stored in the template library.

Without any docking devices, the palm location in each palmprint image may contain some intentional or unintentional disturbances. To alleviate the disturbance effects on the verification process, we utilize 15 subPPIs captured from the same person and compute their averages (Eq. (10)) as the templates.

$$T_j = \sum_{i=1}^{k} \frac{P_{i,j}}{k}, \quad (10)$$

where k is the number of averaged subPPIs, which is 15 in our work, $P_{i,j}$ is the ith subPPI of the jth person and T_j is the template of the jth person.

(2) *Updating stage*: it is used for the verified persons with palmprint template already being stored.

Palmprints will vary while people are growing older. The Kalman predictor [33] is known to possess prediction capabilities. In our approach, we adopt the Kalman predictor with one-step prediction to update the verified template and predict the future template. It will enable the approach to alleviate the variations in palmprints over time. To reduce the amount of computation associated with the Kalman predictor, we select the predictor gain to be a constant α and both of the system parameter and the measurement parameter to be equal to one. The equation of the Kalman predictor is simplified as in Eq. (11).

$$\hat{T}(k+1) = \alpha T_{new}(k) + (1-\alpha)T(k), \quad (11)$$

where $T(k)$ denotes the template library for the kth verification, $T_{new}(k)$ is the verified template at the kth verification, $\hat{T}(k+1)$ is the predicted template for the next verification, and α is the predictor gain with $0 < \alpha < 1$.

Palmprint features are first calculated during the enrollment stage and stored at the template library for verification. In our work, template matching with a correlation function is employed to measure the similarity between the stored template and the new palmprint. The verified palmprint image is then updated to the template library. The predictor gain α is selected according to the period of palmprint variations. Since the collection period of database is too short to generate obvious palmprint variations, we cannot verify the performance of the updating stage and the influence of predictor gain α currently.

7. Verification

We adopt a correlation function to compute the correlation value between the unknown palmprint image and some templates in the template library to verify whether they are captured from the same person or not. There are many mathematical computations for correlation function as described in the literature. The normalized version of the correlation function [34,35] demonstrates the best results for the present application.

$$C_j = \frac{\sum_{r=1}^{m}\sum_{c=1}^{n}(T_j(r,c)-\overline{T_j}(r,c))(Y(r,c)-\overline{Y}(r,c))}{\sqrt{\left(\sum_{r=1}^{m}\sum_{c=1}^{n}(T_j(r,c)-\overline{T}_j(r,c))^2\right)\left(\sum_{r=1}^{m}\sum_{c=1}^{n}(Y(r,c)-\overline{Y}(r,c))^2\right)}}, \quad (12)$$

where m and n are the row and column sizes, respectively, T_j is the template of the jth person in the template library and $\overline{T_j}$ is its mean, Y is the template of the testing palmprint and $\overline{Y}$ is its mean, and C_j denotes the correlated value of T_j and Y. C_j can then be utilized to judge whether a palmprint under test is verified or not.

8. Experimental results

The total number of palmprint images used in our experiment was 4800, which were collected from 160 persons each with 30 palmprint images captured at three different times. The size of each palmprint image was 800×800 with 100 dpi resolution and 256 gray-levels. The data were split into equal parts for each different handpalm. The first acquired 15 images were used as the template images set and the 15 images acquired afterwards were taken as the test set. There were a total of 2400 palmprint images used in constructing 160 templates for the template library. Another

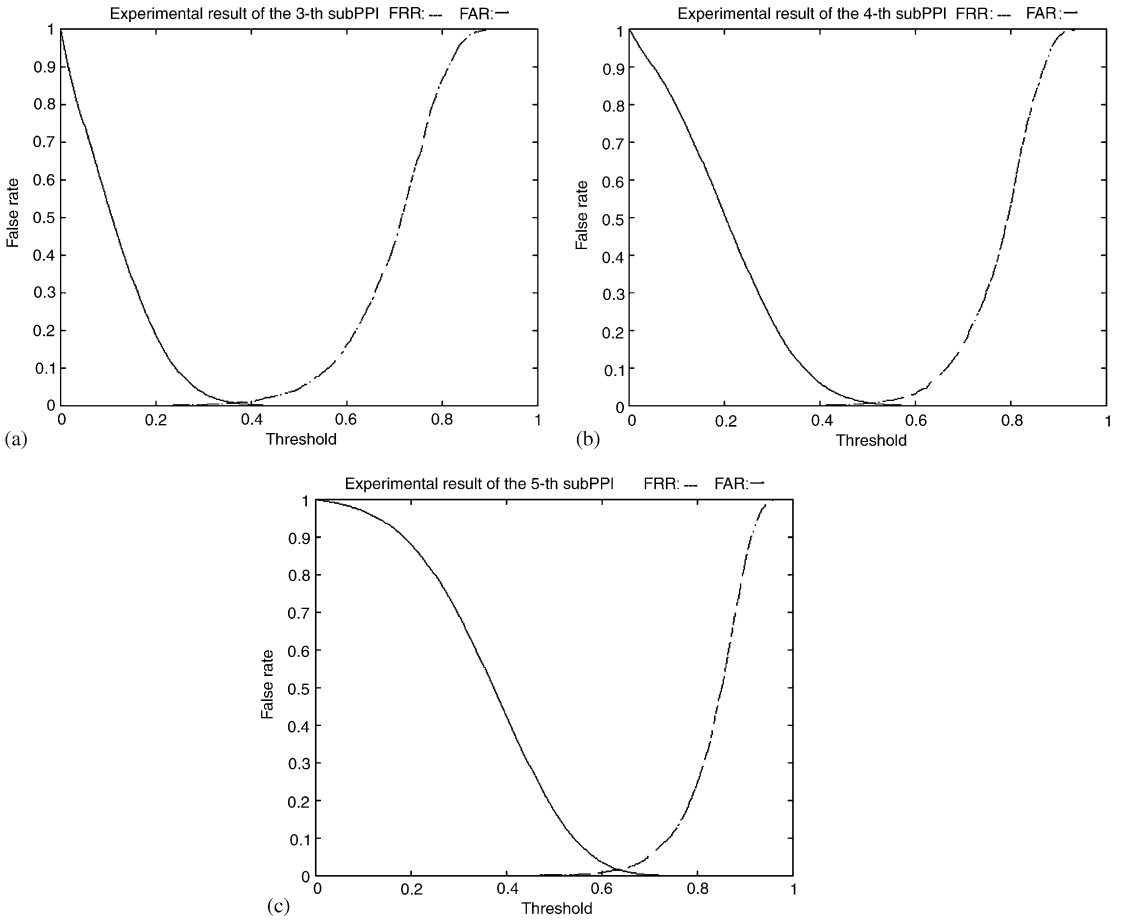

Fig. 11. FAR and FRR of verification results with three different scales of subPPIs. The vertical and horizontal axes represent the false rate and threshold, respectively. (a) the 3rd level subPPI verification result, (b) the 4th level subPPI verification result, (c) the 5th level subPPI verification result.

2400 palmprint images were used as the testing images to verify the validity of the proposed approach.

We adopted the statistical pair known as FRR and FAR to evaluate the performance of the experimental results. In the experiment, the correlation threshold value was set to be R and three different scales were tested and compared. The results with the various thresholds R and false rates are shown in Fig. 11. The experimental results near the cross-over point of FAR and FRR curves (see Fig. 11) are tabulated in Table 1. The threshold at the cross-over point (boldface in Table 1) of FAR and FRR curves is the compromise between FAR and FRR. It is selected as follows.

$$ERR(R) = max\{FAR(R), FRR(R)(R)\}, \tag{13}$$

$$ERR_{co} = min\{ERR(R)\}, \tag{14}$$

$$R_{co} = \{R|ERR(R) = ERR_{co}\}, \tag{15}$$

where $FAR(R)$ and $FRR(R)$ are the error functions of FAR and FRR, respectively, ERR_{co} is the error rate at the cross-over point, and R_{co} is the threshold at the cross-over point.

In high security access control systems, the threshold can be selected larger than 0.74, 0.63 and 0.51 for the 3rd, 4th and 5th level subPPIs, respectively. They achieve zero FAR and acceptable FRR. On the contrary, the threshold can be selected less than 0.47, 0.35 and 0.23 for the 3rd, 4th and 5th level subPPIs, respectively, in low security applications. They will achieve zero FRR and acceptable FAR excepting the 4th level subPPIs.

Failure verifications occur in some palmprint images. They can be categorized into three main groups by carefully observing these failure palmprint images.

(1) Great variation in pressure on scanner from palms while acquiring palmprint images will result in high gray-level (white) region under high pressure as shown in Fig. 12(a). Inside the region, some principal palmprint features may be lost. Moreover, the border of the regions could form pseudo principal palmprint features. These problems might

Table 1
Experimental results near cross-over points (boldface) in Fig. 11

Threshold	FAR(%)	FRR(%)
(a) *the 3rd level subPPI verification result*		
0.23	11.73	0.00
0.27	6.04	0.13
0.31	2.78	0.37
0.37	**0.75**	**0.75**
0.39	0.41	1.00
0.43	0.12	1.92
0.47	0.00	3.04
0.51	0.00	5.17
(b) *the 4th level subPPI verification result*		
0.35	12.66	0.00
0.39	7.29	0.08
0.43	3.82	0.17
0.47	1.85	0.37
0.51	**0.69**	**0.75**
0.55	0.27	1.50
0.59	0.08	2.50
0.63	0.00	4.75
(c) *the 5th level subPPI verification result*		
0.47	24.60	0.00
0.51	15.30	0.13
0.55	9.45	0.33
0.59	4.92	0.58
0.64	**1.62**	**1.62**
0.66	0.72	2.67
0.70	0.18	5.50
0.74	0.00	10.04

lead to mismatching. However, this is a rare and extreme case.

(2) Sometimes palms move when pressing on the scanner which will result in some creases as shown in Fig. 12(b). If these creases are obvious enough, they will form some pseudo palmprint features that do not appear in the template library, which will also result in verification failure.

(3) As shown in Fig. 12(c), some palmprints were too blurry to be distinguished. Too few principal palmprint features were extracted for verification which resulted in verification failure as well.

The conditions (1) and (2) mentioned above can be easily avoided by positioning the palm on the scanner with care while acquiring palmprint images. It is difficult to distinguish the palmprints in condition (3) by applying our approach. This problem can be alleviated by utilizing other methods to extract palmprint features, or combining with other biometric verification methods.

Comparing with the surveyed techniques [8–18] for palmprint classification or verification, our approach applies hierarchical decomposition which includes direction and multi-resolution decompositions to extract principal palmprint features. Then, we adopt a normalized correlation function to match the templates and testing samples. Table 2 summarizes the results generated by our approach and the other techniques [8–18], which are referring to different palmprint databases. As shown in the table, our approach compares very favorably with that of others.

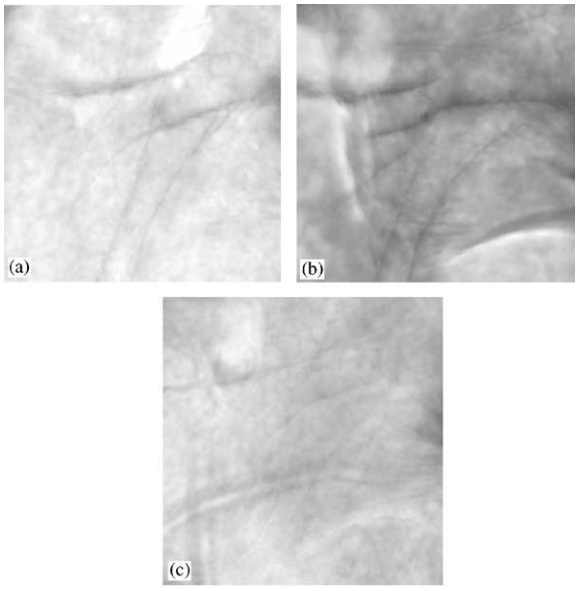

Fig. 12. Examples of failure verification: (a) Palmprint image with some high gray-level ranges. (b) Palmprint image with some pseuod-palmprint (creases). (c) Palmprint image with blur palmprint.

9. Conclusions

In this paper, we present a reliable and robust biometric-based verification approach by using palmprints. There are three main advantages of our proposed approach. The first is that no docking devices and inked palms are needed while acquiring palmprint images. The scanning system is a complete and compact system which provides uniform and consistent image quality due to consistency of the light source, the sensor and the scanning geometry. It is also demonstrated that the training and on-site image taking habits are consistent. These features make a flatbed scanner superior to a video or a digital camera system. Second, the hierarchical decomposition mechanism utilized to effectively extract the principal palmprint features is another advantage. The third advantage is that no prior knowledge about the objects is necessary and the parameters can be set automatically. The algorithm for automatically detecting the four finger-webs location has been tested on 4800 palmprint images captured from 160 different persons. The results show that our technique conforms to the results of manual

Table 2
A comparison of different palmprint verification results

Paper reference	Database		FAR (%)	FAR(%)	Accurate rate(%)
	Number of images	Number of persons			
[8]	108	27	0	0.997	
[9]	100				95
[10]	40	20			95
[11]	425	95	0.37	0.65	
[12]	450	50			97.2
[13]	492	246			94.3
[14]	200	100			95
[15]	3056	191			99.149
[16]	1500	50	0.96	0.5	
[17]	200	100			94
[18]	1000	100	4.49	2.04	
Our proposed approach	4800	160	0.69	0.75	

estimation. We also demonstrate that the use of finger-webs as the datum points to define ROIs is reliable and reproducible. Under normal conditions, the ROIs should cover almost the same region in different palmprint images. Within the ROI, obvious principal palmprint features are extracted by applying the directional decomposition which consists of edge detectors, iterative threshold selection and sequential morphological operators. They are then decomposed into three level multi-resolutions by a multi-resolution analysis with a MRF employed to construct the template library. Any new palmprint features are matched with those from the template library by the template correlation algorithm to verify the identity of the person. Experimental results demonstrate that the proposed approach can obtain acceptable verification accuracy. Such an approach can be applied in access control systems. In high-security demanded applications, very low FAR (even zero) and FRR (acceptable) are mandatory. It is a conflict to reduce both FAR and FRR by using the same biometric feature simultaneously. In order to reduce FAR without increasing FRR, we can combine our techniques with those using palm geometric shapes, finger creases and other biometric features for verification in future research.

Acknowledgements

We acknowledge the support for this study through grants from National Science Council (NSC 93-2622-E-238-012-CC3).

References

[1] A.K. Jain, R. Bolle, S. Pankanti, Biometrics Personal Identification in Networked Society, Kluwer Academic Publishers, Massachusetts, 1999.

[2] Y. Yoshitomi, T. Miyaura, S. Tomita, S. Kimura, Face identification thermal image processing, Proceeding 6th IEEE International Workshop on Robot and Human Communication, RO-MAN' 97 SENDAI.

[3] J.M. Cross, C.L. Smith, Thermographic imaging of the subcutaneous vascular network of the back of the hand for biometric identification, Institute of Electrical and Electronics Engineers 29th Annual 1995 International Carnahan Conference, 1995, pp. 20–35.

[4] B. Miller, Vital sign of identify, IEEE Spectrum 31 (2) (1994) 22–30.

[5] A. Jain, L. Hong, R. Bolle, On-line fingerprint verification, IEEE Trans. Pattern Anal. Mach. Intell. 19 (1997) 302–313.

[6] L. Coetzee, E.C. Botha, Fingerprint recognition in low quality images, Pattern Recogn. 26 (1993) 1441–1460.

[7] C.C. Han, P.C. Chang, C.C. Hsu, Personal identification using hand geometry and palm-print, Fourth Asian Conference on Computer Vision (ACCV), 2000, pp. 747–752.

[8] H.J. Lin, H.H. Guo, F.W. Yang, C.L. Chen, Handprint Identification Using Fuzzy Inference, The 13th IPPR Conference on Computer Vision Graphics and Image Processing, 2000, pp. 164–168.

[9] D. Zhang, W. Shu, Two novel characteristics in palmprint verification: datum point invariance and line feature matching, Pattern Recogn. 32 (1999) 691–702.

[10] J. Chen, C. Zhang, G. Rong, Palmprint recognition using crease, International Conference on Image Processing, vol. 3, 2001, pp. 234–237.

[11] W.K. Kong, D. Zhang, Palmprint texture analysis based on low-resolution images for personal authentication, 16th International Conference on Pattern Recognition, vol. 3, 2002, pp. 807–810.

[12] X. Wu, K. Wang, D. Zhang, Fuzzy directional element energy feature (FDEEF) based palmprint identification, 16th International Conference on Pattern Recognition, vol. 1, 2002, pp. 95–98.

[13] N. Duta, A.K. Jain, K.V. Mardia, Matching of palmprints, Pattern Recogn. Lett. 23 (4) (2002) 477–485.

[14] J. You, W. Li, D. Zhang, Hierarchical palmprint identification via multiple feature extraction, Pattern Recogn. 35 (4) (2002) 847–859.
[15] G. Lu, D. Zhang, K. Wang, Palmprint recognition using eigenpalms features, Pattern Recogn. Lett. 24 (9–10) (2003) 1463–1467.
[16] C.C. Han, H.L. Cheng, C.L. Lin, K.C. Fan, Personal authentication using palmprint features, Pattern Recogn. 36 (2) (2003) 371–381.
[17] W. Li, D. Zhang, Z. Xu, Image alignment based on invariant features for palmprint identification, Signal Process.: Image Commun. 18 (5) (2003) 373–379.
[18] A. Kumar, D.C.M. Wong, H.C. Shen, A.K. Jain, Personal Verification Using Palmprint and Hand Geometry Biometric, in: Proceedings of 4th International Conference on Audio- and Video-Based Biometric Person Authentication (AVBPA), 9–11 June, 2003, pp. 668–678.
[19] X.Z Wang, H.W. Yang, M.H. Zhao, J. Sun, A decision tree based on hierarchical decomposition, International Conference on Machine Learning and Cybernetics, vol. 4, November 2002, pp. 1824–1828.
[20] G. Borgefors, G. Ramella, G. Sanniti Di Baja, Hierarchical decomposition of multiscale skeletons, IEEE Trans. Pattern Anal. Mach. Intell. 23 (11) (2001) 1296–1312.
[21] E. Sharon, A. Brandt, R. Basri, Fast multiscale image segmentation, IEEE Conference on Computer Vision and Pattern Recognition, vol. 1, 13–15 June 2000, pp. 70–77.
[22] H. Rom, G. Medioni, Hierarchical decomposition and axial shape description, IEEE Computer Society Conference on Computer Vision and Pattern Recognition, CVPR'92., 15–18 June 1992, pp. 49–55.
[23] M. Sonka, V. Hlavac, R. Boyle, Image Processing, Analysis, and Machine Vision, second ed., PWS publishing, New York, 1999.
[24] S. Mallat, Multifrequency channel decompositions of images and wavelet models, IEEE Trans. Acoust. Speech, Signal Process. Assp-37 (12) (1989) 2091–2110.
[25] R.C. Gonzalez, R.E. Woods, Digital Image Processing, Addison-Wesley, Reading MA, 1993.
[26] P.S. Wu, M. Li, Pyramid edge detection based on stack filter, Pattern Recogn. Lett. 18 (1997) 239–248.
[27] J. Yoo, E.J. Coyle, C.A. Bouman, Dual stack filters and the modified difference of estimates approach to edge detection, IEEE Trans. Image Process. 6 (1997) 1634–1645.
[28] J. Yoo, C.A. Bouman, E.J. Delp, E.J. Coyle, The nonlinear prefiltering and difference of estimates approaches to edge detection: Applications of stack filters, Computer Vision Graph. 55 (2) (1993) 140–159.
[29] J. Koenderink, The structure of images, in: Biological Cybernetics, Springer, New York, 1984.
[30] Y. Shinagawa, T.L. Kunil, Unconstrained automatic images matching using multiresolutional critical-point filter, IEEE Trans. Pattern Anal. Mach. Intell. 20 (1998) 994–1010.
[31] Y. Qi, B.R. Hunt, A multiresolution approach to computer verification of handwritten signatures, IEEE Trans. Image Process. 4 (1995) 870–874.
[32] J. You, P. Bhattacharya, A wavelet- based coarse-to-fine image matching scheme in a parallel virtual machine environment, IEEE Trans. Image Process. 9 (2000) 1547–1559.
[33] S.M. Bozic, Digital and Kalman Filtering, Edward Arnold, London, 1979.
[34] K.S. Fu, R.C. Gonzalez, C.S.G. Lee, Robotics: Control, Sensing, Vision and Intelligence, McGraw-Hill, New York, 1987 pp. 426–427.
[35] M.R. Spiegel, Theory and Problems of Probability and Statistics, Schaum's Outline Series, McGraw-Hill, New York, 1988.

About the author—CHIH-LUNG LIN was born on 15 January 1965 in Tainan, Taiwan, ROC. He received his Ph.D. in Institute of Computer Science and Information Engineering at National Central University in 2003. He was an assistant researcher in the Chung-Sun Institute of Science and Technology (CSIST), Lung-Tan, Taiwan in 1989. His current research interests include biometrics authentication, pattern recognition, image processing and fiber communication.

About the author—THOMAS C. CHUANG was born on Dec 5, 1954 in Taiwan, ROC. He received his Ph.D. degrees in Electrical Engineering from the University of California, Los Angles in 1981. He has worked for many internationally well-known companies like Eastman Kodak, DuPont and Raytheon. He joined Vanung University as an Associated Professor in the Department of Computer Science and Information Engineering in 2002. His current research interests include image processing, pattern recognition, natural language processing, neural network and system automation.

About the Author—KUO-CHIN FAN was born in Hsinchu, Taiwan, on 21 June 1959. He received his B.S. degree in Electrical Engineering from National Tsing-Hua University, Taiwan, in 1981. In 1983, he worked for the Electronic Research and Service Organization (ERSO), Taiwan, as a Computer Engineer. He received his graduate degree in Electrical Engineering at the University of Florida in 1984 and received the M.S. and Ph.D. degrees in 1985 and 1989, respectively. From 1984 to 1989 he was a Research Assistant in the Center for Information Research at University of Florida. In 1989, he joined the Institute of Computer Science and Information Engineering at National Central University where he became a professor in 1994. From 1994 to 1997 he was chairman of the department. Currently, he is the director of the Computer Center. He is a member of IEEE and SPIE. His current research interests include image analysis, optical character recognition, and document analysis.